Journal of Power Sources 288 (2015) 296–301

Contents lists available at ScienceDirect

Journal of Power Sources

journal homepage: www.elsevier.com/locate/jpowsour

Greatly improved electrochemical performance of lithium–oxygen batteries with a bimetallic platinum–copper alloy catalyst

Minwook Lee, Yubin Hwang, Kyung-Han Yun, Yong-Chae Chung*

Department of Materials Science and Engineering, Hanyang University, Seoul 133-791, Republic of Korea

HIGHLIGHTS

- Li–O_2 reactions are investigated on Pt–Cu alloy catalysts using DFT calculation.
- PtCu (111) has greatly reduced overpotentials, η_C = 0.49 V and η_{DC} = 0.26 V.
- Inherent surface charge of alloy catalyst mainly affects η of Li–O_2 battery.
- Pt-based alloys have general rule for Li–O_2 reactions decided by surface charge.

GRAPHICAL ABSTRACT

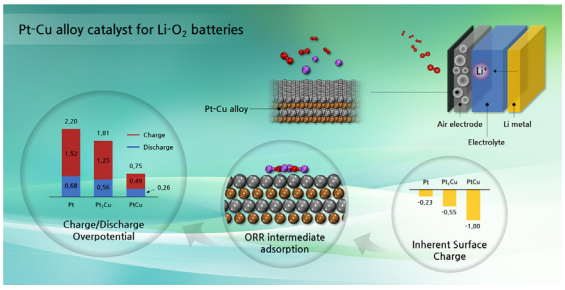

ARTICLE INFO

Article history:
Received 22 December 2014
Received in revised form
16 April 2015
Accepted 22 April 2015
Available online 25 April 2015

Keywords:
Lithium–oxygen batteries
Platinum–copper alloy catalyst
Oxygen reduction reaction
Surface charge
Density functional theory

ABSTRACT

Research on the cathode catalysts of lithium–oxygen (Li–O_2) batteries is one of the most important branches to commercialize these batteries to overcome the sluggish kinetics during both the oxygen reduction reaction (ORR) and the oxygen evolution reaction (OER). In this study, a high performance catalyst based on a bimetallic Pt–Cu alloy is investigated for Li–O_2 batteries using first-principles calculation. The theoretical prediction shows that the Pt–Cu alloy is much more effective than the pure Pt according to the electrochemical performance. In particular, the effectiveness of the catalytic property is maximized in the case of the PtCu (111) surface which greatly reduces the large overpotentials of the original Li–O_2 batteries during the OER/ORR. It is identified for the first time that the charge overpotentials are affected mainly by the inherent surface charge character of the alloy catalyst. It is observed that the more negatively charged PtCu (111) surface can act as a weakly positively charged surface for the adsorption of Li–O intermediates and thus result in weak ionic bonding of the intermediates on the surface. As a result, the dominant factor improving the catalytic performance is clearly demonstrated, providing insight into the design of an efficient catalyst for Li–O_2 battery technologies.

1. Introduction

The lithium–oxygen (Li–O_2) battery has recently attracted a great deal of attention as a promising power source for all-electric vehicles as it has the highest theoretical energy density (3458 Wh kg^{-1} in non-aqueous electrolyte) among next generation rechargeable batteries [1–5]. Considering the practical situations, the energy density of Li–O_2 battery is expected to 1000 Wh kg^{-1}, comparable to the tank-to-wheel energy density of gasoline (1750 Wh kg^{-1}) [5,6]. However, the low round-trip energy efficiency in practical employment is one of the biggest obstacles to the

* Corresponding author.
E-mail address: yongchae@hanyang.ac.kr (Y.-C. Chung).

http://dx.doi.org/10.1016/j.jpowsour.2015.04.143
0378-7753/

commercialization of Li–O_2 batteries [7–9]. It is well known that the problem of low round-trip efficiency stems from the overpotentials during both the oxygen evolution reaction (OER, on charging) and the oxygen reduction reaction (ORR, on discharging) at the O_2 diffusion cathodes [8–10]. In particular, substantially larger overpotentials are observed during the OER compared to the ORR, which fatally exacerbates the kinetics of the Li–O_2 batteries [11,12]. Hence, an effective cathode catalyst is essential to improve the nature of the large overpotentials during the OER.

Among the recent studies of cathode catalysts for Li–O_2 batteries [13–27], one of the most promising candidates to improve the large overpotentials is the noble metal based alloy catalyst [23–27]. Lu et al. showed that platinum and gold nanoparticles are effective in reducing the charge overpotentials and discharge overpotentials, respectively [10,23]. Moreover, the advantages of each noble metal can be obtained by alloying them together to form a bifunctional catalyst [23]. Another alloying strategy is to combine noble metals with 3*d* transition metals such as Pt–Co [24,25], Pt–Ni [26], and Pd–Cu [27] alloys. Alloying the high-priced noble metals with the much cheaper 3*d* transition metals has an obvious advantage in terms of the economic feasibility for mass production of Li–O_2 battery packs. Furthermore, it was reported that these types of alloy catalysts more effectively lowered the charge overpotentials than pure noble metal catalysts [24–27].

As a non-alloyed noble metal, Pt is one of the most effective catalytic elements for the general ORR mechanism [28], which shows a great reduction of the charge overpotentials of the Li–O_2 batteries [23]. In addition, the Pt–Cu alloy catalyst has also been widely used in other catalytic reactions such as the methanol oxidation reaction [29,30] and the ethanol oxidation reaction [31] owing to its high catalytic property. Recently, Choi et al. reported that Li–O_2 cell performance was improved by using a Cu alloyed Pd catalyst [27]. In light of this perspective, alloying Pt with Cu is expected to show advanced performance as a cathode catalyst for the Li–O_2 battery. However, analysis focusing on the possibility of Pt–Cu alloy catalysts for Li–O_2 battery cathode is still insufficient. Moreover, insight into how the mechanism underlying the catalytic performance can be enhanced by alloying metal has still not been explored in Li–O_2 battery technologies.

In the present study, the electrochemical performance of the Pt–Cu alloy catalyst during both the OER and the ORR of the Li–O_2 batteries is investigated using a first-principles calculation based on density functional theory (DFT). The main purpose of the study is to investigate the initial/final stage of the ORR/OER on the catalytic surface, which is extremely difficult to be confirmed by the experimental observation. Here, the study focuses on the intrinsic catalytic property with respect to the atomic ratio of the metal alloy, thus the effect of the external environment which influences the reaction on the surface was excluded. Theoretically, the Pt–Cu alloy catalyst shows great improvement in the reduction of the overpotential. In particular, there is a dramatic reduction in the charge overpotential for the particular surface structure of the Pt–Cu alloy. The origin of the sharp reduction in the charge overpotential of the Pt–Cu alloy is found through analysis of the Coulomb interaction energies derived from the quantitative charge analysis of the surface layers and adsorbates. Here, it is presented for the first time that the surface charge of the metal alloy could be the most dominant factor affecting the overpotential. All calculations are performed by considering the possible crystallographic order of the Pt–Cu alloy. The correlation of the adsorption strength of the ORR intermediates with the surface charge properties is analyzed to understand how the catalytic behavior was improved on the Pt–Cu alloy. This theoretical study may provide in-depth insight into the design of effective alloy catalysts.

2. Calculation methods

Spin-polarized DFT calculations were carried out using the projector augmented-wave (PAW) method [32], as implemented in the Vienna ab initio simulation package code (VASP) [33]. The Perdew-Burke-Ernzerhof (PBE) within the generalized gradient approximation (GGA) was adopted to examine the electronic exchange-correlation function of the interacting electrons [34]. The Kohn-Sham valance electrons of 1*s*2*s* for Li, 2*s*2*p* for C, and O, 3*d*4*s* for Cu, and 5*d*6*s* for Pt were expended on a plane wave basis set to a kinetic cutoff energy of 400 eV. The Brillouin zone was sampled using a $12 \times 12 \times 12$ and a $3 \times 3 \times 1$ *k*-point mesh generated by the Γ-centered Monkhorst-Pack scheme [35] for unitcell and surface calculations, respectively. The Brillouin zone integrations were performed with the Methfessel-Paxton (MP) smearing method [36] with a broadening width of 0.1 eV. All of the self-consistent loops were iterated until the total energy difference of the systems between the adjacent iterating steps was less than 10^{-5} eV. The modeled structures were fully relaxed until the Hellman-Feynman forces were in a range of ±0.02 eV $Å^{-1}$.

Among the typical combinations of the Pt–Cu alloys (Pt_3Cu, PtCu, and $PtCu_3$), the surface models were designed for the possibility of making a Pt-skin surface since the 3*d* transition metal atoms at the topmost layer would decrease the catalytic activity of the Li–O_2 batteries [27]. Thus, a Pt-skinned Pt_3Cu surface with an $L1_2$ order [37,38] and a Pt-terminated PtCu surface with an $L1_1$ order [39] were considered as representatives of the Pt–Cu alloy catalyst. A $PtCu_3$ with the $L1_2$ order was not considered since its high proportion of Cu hinders formation of the Pt-skin surface. In addition, a pure Pt surface was modeled as the standard point for the catalytic activity of the pure noble metal. Since Pt, Pt_3Cu, and PtCu have face-centered cubic (fcc) or fcc-like closed-packed structures, adsorption of the ORR intermediates (LiO_2, Li_2O_2, and $(Li_2O)_2$) was calculated on the thermodynamically most stable (111) plane. The lateral lattice parameters of Pt (111), Pt_3Cu (111), and PtCu (111) were 2.81 Å, 2.76 Å, and 2.74 Å, respectively. Each surface model consists of four layers of the metal atoms (Pt, Cu) where the bottommost layer was fixed to keep the bulk property and the upper layers were fully relaxed according to the above-mentioned relaxation condition. To avoid a direct interaction between the periodic images [40], the surface models were designed by taking a 4×4 supercell and a vacuum spacing of 15 Å to the normal direction. The relaxed 4×4 surface models of Pt (111), Pt_3Cu (111), and PtCu (111) are shown in Fig. S1.

Free energy diagrams were achieved by the most stable adsorption configuration of the ORR intermediates among all the possible configurations. The adsorption of the ORR intermediates was conducted on the clean Pt-skin surface to confirm the initial reaction of the ORR and the final reaction of the OER, where the role of the catalytic surface becomes significant. The Gibbs free energies of the ORR intermediates in the electrochemical reaction pathways were calculated using Eq. (1):

$$\Delta G = \Delta E^{\mathrm{Total}} + \Delta E^{\mathrm{ZPE}} - T\Delta S \quad (1)$$

where $\Delta E^{\mathrm{Total}}$, ΔE^{ZPE}, and ΔS denote the change of the DFT total energy, zero-point energy, and the entropy at T = 298.15 K, respectively. The values of ΔE^{ZPE} and ΔS of the ORR intermediates were calculated from the vibrational frequencies obtained by using a widely used method for the DFT calculations. The free energy of a solvated Li^+ ion and an electron (e^-) were set in equilibrium with a bulk Li [41], and the free energy of the gas phase of the O_2 molecule was calculated from the free energies of H_2O, H_2, and the experimental formation enthalpy of H_2O ($\Delta H^\circ_f = -241.83$ kJ mol^{-1}) [19,41]. The effect of the applied voltage was reflected by shifting

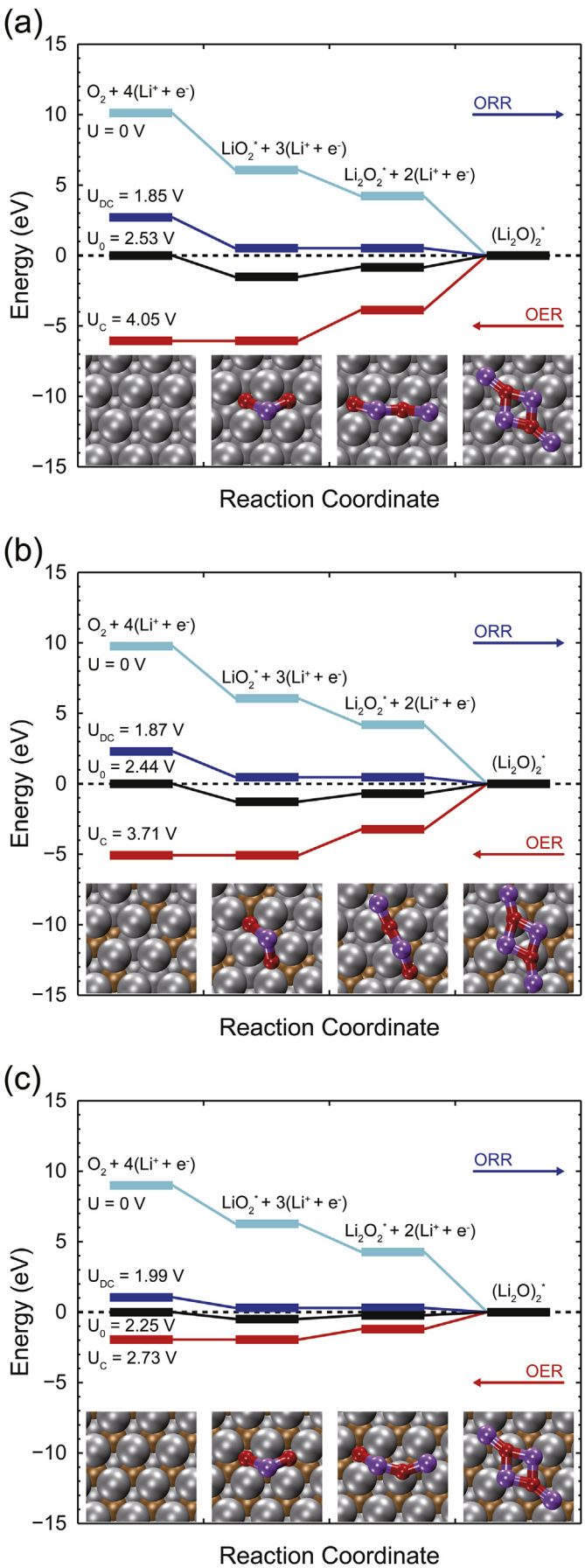

ΔG to $-neU$, where n is the number electrons transferred, e is the elementary positive charge, and U is the applied voltage. The adsorption energies of the ORR intermediates on the surface models were calculated using Eq. (2):

$$E_{ads} = -\left[E_{Li_xO_2/surface} - E_{Li_xO_2} - E_{surface}\right] \quad (2)$$

where $E_{Li_xO_2/surface}$, $E_{Li_xO_2}$, and $E_{surface}$ denote the DFT total energies of the surface with the adsorbed ORR intermediates, free ORR intermediates, and relaxed surface structure, respectively.

3. Results and discussion

The overall reactions occurring at the O_2 diffusion cathodes of the non-aqueous Li–O_2 batteries are known for (*i*) $2(Li^+ + e^-) + O_2 \leftrightarrow Li_2O_2$ (a two-electron pathway), and (*ii*) $4(Li^+ + e^-) + O_2 \leftrightarrow (Li_2O)_2$ (a four-electron pathway) [42]. According to Lu et al., the reaction pathway of the Li–O_2 batteries is strongly governed by the ability to dissociate the O_2 molecule on the catalytic surfaces [10]. When the dissociation of the O_2 molecule is easy, such as on the Pt surface, the reaction prefers to progress through the four-electron pathway. Furthermore, it was shown that the four-electron pathway is a spontaneous reaction on the surface of the noble metals (Pd, and Pt) and their alloys (PdCu, and Pt_3Co) [19,25,27]. In the case of the Pt–Cu alloy surfaces, their reaction pathways are expected to show an analogous behavior to the Pt_3Co surface since both the Pt–Cu surfaces and the Pt_3Co surface have a similar structure such as the Pt-skin surface and the close-packed structure. Hence, the free energy diagrams were obtained through the four-electron pathway on the Pt–Cu alloy surfaces, where the adsorption of the $(Li_2O)_2$ molecule and the intermediates (LiO_2, Li_2O_2) were performed with the most stable adsorption configurations.

Fig. 1 shows the free energy diagrams along the OER and the ORR pathways with the most stable adsorption configurations of the ORR intermediates on the Pt (111), Pt_3Cu (111), and the PtCu (111) surfaces. Note that the adsorption geometries are identical regardless of the surface types. Each reaction pathway consists of the following three elementary reaction steps: (*i*) $4(Li^+ + e^-) + O_2 \leftrightarrow LiO_2^* + 3(Li^+ + e^-)$, (*ii*) $LiO_2^* + 3(Li^+ + e^-) \leftrightarrow Li_2O_2^* + 2(Li^+ + e^-)$, and (*iii*) $Li_2O_2^* + 2(Li^+ + e^-) \leftrightarrow (Li_2O)_2^*$ where the asterisk marks the adsorbed states of the molecules. To confirm the electrochemical performance on each surface, the charge voltages (U_C) and discharge voltages (U_{DC}) were obtained as the minimum and the maximum voltage, which makes each pathway remain downhill. It can be seen that the Pt_3Cu (111) surface has better performance than the pure Pt (111) surface (see Fig. 1a and b). Here, the U_C of the Pt_3Cu (111) surface shows a distinct improvement with a much lower voltage of 3.71 V than the U_C of the Pt (111) surface (4.05 V). The U_{DC} of the Pt_3Cu (111) surface is also improved compared to the Pt (111) surface; however, the degree of improvement is negligible compared to the improvement of U_C. In the case of the PtCu (111) surface, the best electrochemical performance was observed among all of the calculated surfaces (see Fig. 1c). In particular, the U_C of the PtCu (111) surface improved remarkably with the lowest voltage of 2.73 V compared to the U_C of

Fig. 1. Free energy diagrams for the OER/ORR on (a) Pt (111), (b) Pt_3Cu (111), and (c) PtCu (111) surfaces at the zero potential (U = 0 V), minimum charge potential (U_C), maximum discharge potential (U_{DC}), and the equilibrium potential (U_0), respectively. Each diagram consists of the most stable adsorption configurations of the ORR intermediates (LiO_2, Li_2O_2, and $(Li_2O)_2$). Purple, red, gray, and brown balls denote the Li, O, Pt, and Cu atoms. (For interpretation of the references to colour in this figure legend, the reader is referred to the web version of this article.)

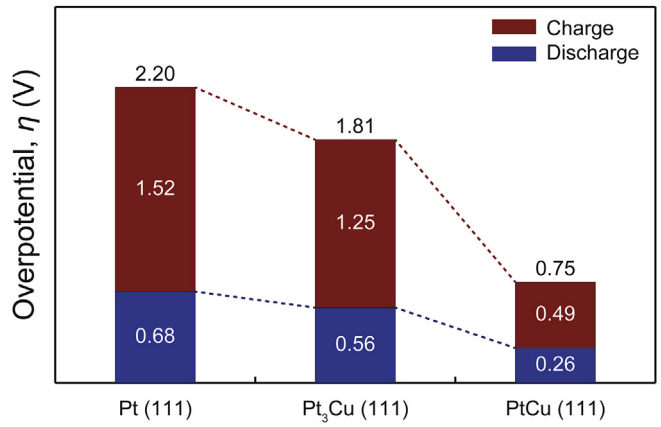

Fig. 2. The calculated charge overpotentials (η_C), discharge overpotentials (η_{DC}), and the total overpotentials (η_{Total}) on the Pt (111), Pt_3Cu (111), and PtCu (111) surfaces. The red and blue bars denote η_C and η_{DC}, and the η_{Total} is stated above the stacked bars. (For interpretation of the references to colour in this figure legend, the reader is referred to the web version of this article.)

the Pt_3Cu (111) as well as the pure Pt (111) surfaces. Furthermore, improvement of the U_{DC} on the PtCu (111) surface becomes more obvious with the highest voltage of 1.99 V as compared to the negligible change on the Pt_3Cu (111) surface.

To investigate how much this improvement in the electrochemical performance corresponds to the catalytic efficiency of the Pt–Cu alloy surfaces, the overpotentials are achieved as illustrated in Fig. 2. The charge overpotential (η_C), discharge overpotential (η_{DC}), and the total overpotential (η_{Total}) are calculated as (*i*) $\eta_C = U_C - U_0$, (*ii*) $\eta_{DC} = U_0 - U_{DC}$, and (*iii*) $\eta_{Total} = \eta_C + \eta_{DC}$, respectively. The η_{Total} was gradually reduced in accordance with an increment in the Cu/Pt atomic ratio. In other words, alloying the Pt with the Cu is obviously effective in the Cu range of 0–0.5. In particular, reduction of the η_{Total} is remarkably sharp in the case of the PtCu (111) surface (0.75 V) as compared to the η_{Total} of the Pt_3Cu (111) (1.81 V) and the Pt (111) (2.20 V) surfaces. Furthermore, a large proportion of this remarkable η_{Total} reduction on the PtCu (111) surface is accomplished mainly by the reduction of the η_C, while the reduction of the η_{DC} constitutes only a rather low proportion. The dominant reduction of the η_C compared to the η_{DC} is also observed in the case of the other noble metal based alloy catalysts [25,27], which implies that this tendency is a general feature of noble metal based alloy catalysts. When the PtCu (111) surface is compared with the other alloy surfaces such as PdCu (111) and Pt_3Co (111) [25,27], it can be seen that the η_{Total} of the PtCu (111) surface also has a substantially smaller value (see Table S1). Although there are some differences in the calculation details between these studies, the smallest η_{Total} of the PtCu (111) surface is sufficiently meaningful to indicate great improvement of the catalytic efficiency. According to the overpotentials calculated from the free energy diagrams, it is obvious that alloying the Pt with the Cu is substantially effective, especially in the case of the PtCu (111) surface. However, it is still unclear why the reduction of the η_C is much larger than the reduction of the η_{DC} for the PtCu (111) surface.

Considering that the free energy of each reaction step (G_i) is potential dependent and is thus shifted by U times the number of the coupled Li ions and electrons ($Li^+ + e^-$), the reaction step with the maximum energy difference among all the reaction steps is the determining step of the U_C ($U_C = \max[-\Delta G_i/e]$) [41,43]. As shown in the free energy diagrams (Fig. 1), the U_C of the Pt–Cu surfaces is determined in the final steps of the OER pathway. Since the free energies of the free O_2 molecules and the free Li ions are independent of the surface types, the U_C is solely dependent on the adsorbed state of the LiO_2 molecules. In the case of the U_{DC}, however, the U_{DC} is determined during the reaction step with the minimum energy difference ($U_{DC} = \min[-\Delta G_i/e]$) [41,43], and thus the second steps of the ORR pathway determine the U_{DC} in the free energy diagrams for Pt–Cu surfaces (Fig. 1). In other words, the U_{DC} is determined by the difference in the adsorption strength between the Li_2O_2 and the LiO_2 intermediates. These mechanisms for determining the steps of the OER and the ORR are analogous to the case of the other metal alloy catalysts [25,27].

To confirm the accurate meanings of the adsorbed states in the case of the Pt–Cu alloy surfaces, the adsorption energies (E_{ads}) of the ORR intermediates are calculated as listed in Table 1. The E_{ads} of all the ORR intermediates were gradually decreased according to the increment of the Cu/Pt ratio. Above all, the E_{ads} of the LiO_2 molecule, which solely determines the U_C, decreased with the largest variance. Furthermore, it can be seen that the E_{ads} of the LiO_2 molecule is weakest on the PtCu (111) surface. As compared with the Pt (111) and the Pt_3Cu (111) surfaces, the PtCu (111) surface has a weaker E_{ads} of the LiO_2 molecule, which is about more than 1 eV. Owing to this weakest E_{ads} of the LiO_2 molecule, the PtCu (111) shows the lowest voltage of U_C, which causes the smallest η_C. On the other hand, the E_{ads} difference between the Li_2O_2 and the LiO_2 molecules, which determines the U_{DC}, varied slightly depending on the surface type since the E_{ads} of the Li_2O_2 molecule and the LiO_2 molecule decrease simultaneously according to the increment of the Cu/Pt ratio. Hence, the U_{DC} showed analogous values regardless of the surface. Although the E_{ads} of all the ORR intermediates is influenced by the alloying Cu, the most meaningful changes occurred at the adsorption of the LiO_2 molecule since it solely determines the U_C with a large variance. Thus, it seems crucial to analyze the adsorption character of the LiO_2 molecule. In this regard, the intrinsic properties of each Pt–Cu surfaces are worth noting for further insight in improving the catalytic efficiency.

The surface characters are compared by surface charge distribution and the Coulomb interaction energies using Bader charge analysis [44,45] as listed in Table 2. When the ORR intermediates of the Li–O_2 batteries are adsorbed on the metal surfaces [25,27] or silicene [46], it is known that the Coulomb interaction between the molecule and the surface layer is a crucial factor to determine the catalytic activity. In other words, the ionic bonding is a major influence in determining the adsorption strength of the ORR intermediates. According to Table 2, the Coulomb interaction energies between the LiO_2 molecules and the surface layers ($-Q_{surf,after}Q_{LiO_2}/H$) gradually decrease in the sequence of the Cu/Pt ratio, which corresponds to the result of the E_{ads}. Furthermore, Fig. 3a complements the E_{ads} of the LiO_2 molecule showing a linear relationship with the Coulomb interaction energy. Here, it is notable that the charge values of ΔQ_{surf} ($Q_{surf,after} - Q_{surf,before}$), Q_{LiO2}, and the heights (H) are independent of the surface types. If the Coulomb interaction energy was restated as $-(Q_{surf,before} + \Delta Q_{surf})Q_{LiO_2}/H$, only the $Q_{surf,before}$ remains as the main factor to determine the Coulomb interaction energy. As illustrated in Fig. 3b, the E_{ads} of the LiO_2 molecule also shows a

Table 1
Adsorption energies (E_{ads}) of the ORR intermediates (LiO_2, Li_2O_2, and $(Li_2O)_2$) on Pt (111), Pt_3Cu (111), and PtCu (111) surfaces.

	E_{ads} (eV)		
	LiO_2	Li_2O_2	$(Li_2O)_2$
Pt (111)	3.29	3.79	5.29
Pt_3Cu (111)	2.93	3.46	4.94
PtCu (111)	1.96	2.58	4.16

Table 2
The calculated charge values, height between the LiO_2 molecule and the surface layer, and the Coulomb interaction energy in the case of LiO_2 molecule adsorption on Pt (111), Pt_3Cu (111), and PtCu (111) surfaces, respectively. The calculated charge values consist of the surface charge before adsorption ($Q_{surf,before}$), surface charge after adsorption ($Q_{surf,after}$), surface charge difference from adsorption (ΔQ_{surf}), charge of the 2nd layer before the adsorption ($Q_{2nd,before}$), and the charge transferred to the LiO_2 molecule (Q_{LiO_2}).

	Charge values (q)					H (Å)	$-Q_{surf,after}Q_{LiO_2}/H$ (q^2/Å)
	$Q_{surf,before}$	$Q_{surf,after}$	ΔQ_{surf}	$Q_{2nd,before}$	Q_{LiO_2}		
Pt (111)	−0.23	0.78	1.08	0.25	−0.79	1.20	0.52
Pt_3Cu (111)	−0.55	0.49	1.14	0.70	−0.84	1.34	0.31
PtCu (111)	−1.00	0.02	1.11	1.70	−0.83	1.31	0.01

linear relationship with the $Q_{surf,before}$. $Q_{2nd,before}$ indicates that the inherent surface charge of the surfaces are different due to the difference in the contained ratio of the Cu atoms in the 2nd layer. It is seen that the more the Cu atoms are contained in the 2nd layer, the more the electrons are transferred to the surface Pt layer, which makes strong negative surface charge inherently. It is inferred that the reason for the larger electron transfer in case of the higher Cu ratio is owing to the large electronegativity difference between Pt (2.28) and Cu (1.90). Thus, the inherent surface charge is most negative in case of PtCu (111) owing to the highest ratio of the Cu atoms. It is an interesting result that the adsorption strength of the metal alloys can be determined only by its inherent surface charge before the adsorption. In the case of ionic bonding such as molecular adsorption on a metal surface, the surface adsorption character

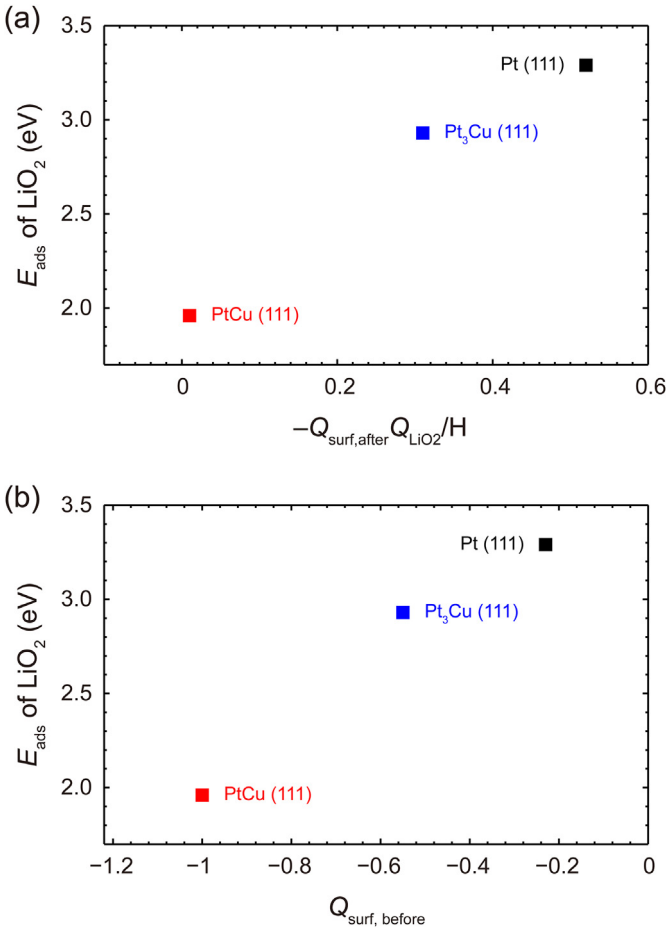

Fig. 3. Adsorption energy of the LiO_2 molecule as a function of (a) the Coulomb interaction energy ($-Q_{surf,after}Q_{LiO2}/H$), and (b) the surface charge before the adsorption ($Q_{surf,\ before}$). The black, blue, and red squares denote the Pt (111), Pt_3Cu (111), and PtCu (111) surfaces, respectively. (For interpretation of the references to colour in this figure legend, the reader is referred to the web version of this article.)

is significantly affected by the surface charge distribution of the catalyst. Since the same amounts of electrons are transferred for each Pt–Cu surface ($\Delta Q_{surf} \approx 1.1$, in Table 2), the PtCu (111) surface shows a relatively weak positive charge after LiO_2 adsorption ($Q_{surf,after} = 0.02$, in Table 2) and therefore indicates the smallest Coulomb interaction energy compared to the other surfaces. In light of the correlation of the surface charge and the adsorption strength, the more negatively charged surface results in weaker adsorption of the LiO_2 intermediates and consequently the U_C is expected to be quite small. Accordingly, the promising catalytic properties of the alloy surfaces might be expected through a check for the surface charge. Although this tendency is still applied to the Pt-based alloy surfaces in light of the studies of the PdCu (111) and Pt_3Co (111) surfaces [25,27], it is expected that other metal based alloy groups with the same surface atoms will show similar patterns of behavior. Therefore, further research is necessary to provide the general properties of the other metal alloy systems.

4. Conclusions

The electrochemical performance of the cathode catalyst for the Li–O_2 battery was theoretically predicted in this DFT calculation. The Pt–Cu alloy, PtCu (111) surface, in particularly, is expected to be the best choice for designing a cathode catalyst and thereby reduces the overpotential more efficiently. In particular, the dramatic reduction of U_C is the main contributor to the reduction of the overall overpotential. The Coulomb interaction energies of the LiO_2 adsorption for each of the surface structures of Pt (111), Pt_3Cu (111), and PtCu (111) were compared to find the mechanism of how the PtCu (111) surface shows outstanding properties compared to the other surfaces. Discussion of the distinctive surface charge character of each surface structure provides the meaningful insight that the more negatively charged metal alloy surface adsorbs the reaction intermediates such as the LiO_2 molecule by moderate attractive force. This change results in the reduction of U_C in the OER process. The result of the present study suggests that the desirable catalytic properties of the Pt-based alloy catalysts can be estimated by the surface charge before adsorption. Moreover, estimation of the catalytic properties could be extended to other noble metal based alloy groups through further analysis of the relation between the surface charge and the adsorption energy.

Acknowledgments

This research was supported by the Basic Science Research Program through the National Research Foundation of Korea (NRF) funded by the Ministry of Education (2013R1A1A2A10064432).

Appendix A. Supplementary data

Supplementary data related to this article can be found at http://dx.doi.org/10.1016/j.jpowsour.2015.04.143.

References

[1] G. Girishkumar, B. McCloskey, A.C. Luntz, S. Swanson, W. Wilcke, J. Phys. Chem. Lett. 1 (2010) 2193–2203.
[2] J.-S. Lee, S.T. Kim, R. Cao, N.-S. Choi, M. Liu, K.T. Lee, J. Cho, Adv. Energy Mater. 1 (2011) 34–50.
[3] P.G. Bruce, S.A. Freunberger, L.J. Hardwick, J.-M. Tarascon, Nat. Mater. 11 (2012) 19–29.
[4] J. Lu, L. Li, J.-B. Park, Y.-K. Sun, F. Wu, K. Amine, Chem. Rev. 114 (2014) 5611–5640.
[5] L. Grande, E. Paillard, J. Hassoun, J.-B. Park, Y.-J. Lee, Y.-K. Sun, S. Passerini, B. Scrosati, Adv. Mater. 27 (2015) 784–800.
[6] J. Christensen, P. Albertus, R.S. Sanchez-Carrera, T. Lohmann, B. Kozinsky, R. Liedtke, J. Ahmed, A. Kojic, J. Electrochem. Soc. 159 (2012) R1–R30.
[7] A. Débart, J. Bao, G. Armstrong, P.G. Bruce, J. Power Sources 174 (2007) 1177–1182.
[8] Y. Shao, S. Park, J. Xiao, J.-G. Zhang, Y. Wang, J. Liu, ACS Catal. 2 (2012) 844–857.
[9] Y.-C. Lu, B.M. Gallant, D.G. Kwabi, J.R. Harding, R.R. Mitchell, M.S. Whittingham, Y. Shao-Horn, Energy Environ. Sci. 6 (2013) 750–768.
[10] Y.-C. Lu, H.A. Gasteiger, E. Crumlin, R. McGuire, Y. Shao-Horn, J. Electrochem. Soc. 157 (2010) A1016–A1025.
[11] Y. Mo, S.P. Ong, G. Ceder, Phys. Rev. B 84 (2011) 205446.
[12] Y.-C. Lu, Y. Shao-Horn, J. Phys. Chem. Lett. 4 (2013) 93–99.
[13] A. Débart, A.J. Paterson, J. Bao, P.G. Bruce, Angew. Chem. 120 (2008) 4597–4600.
[14] J. Li, N. Wang, Y. Zhao, Y. Ding, L. Guan, Electrochem. Commun. 13 (2011) 698–700.
[15] A.K. Thapa, Y. Hidaka, H. Hagiwara, S. Ida, T. Ishihara, J. Electrochem. Soc. 158 (2011) A1483–A1489.
[16] H. Wang, Y. Yang, Y. Liang, G. Zheng, Y. Li, Y. Cui, H. Dai, Energy Environ. Sci. 5 (2012) 7931–7935.
[17] F. Li, R. Ohnishi, Y. Yamada, J. Kubota, K. Domen, A. Yamada, H. Zhou, Chem. Commun. 49 (2013) 1175–1177.
[18] H.-G. Jung, Y.S. Jeong, J.-B. Park, Y.-K. Sun, B. Scrosati, Y.J. Lee, ACS Nano 7 (2013) 3532–3539.
[19] Y. Xu, W.A. Shelton, J. Chem. Phys. 133 (2010) 024703.
[20] J.R. Harding, Y.-C. Lu, Y. Tsukada, Y. Shao-Horn, Phys. Chem. Chem. Phys. 14 (2012) 10540–10546.
[21] B. Sun, P. Munroe, G. Wang, Sci. Rep. 3 (2013) 2247.
[22] J.-J. Xu, Z.-L. Wang, D. Xu, L.-L. Zhang, X.-B. Zhang, Nat. Commun. 4 (2013) 2438.
[23] Y.-C. Lu, Z. Xu, H.A. Gasteiger, S. Chen, K. Hamad-Schifferli, Y. Shao-Horn, J. Am. Chem. Soc. 132 (2010) 12170–12171.
[24] D. Su, H.-S. Kim, W.-S. Kim, G. Wang, J. Power Sources 244 (2013) 488–493.
[25] B.G. Kim, H.-J. Kim, S. Back, K.W. Nam, Y. Jung, Y.-K. Han, J.W. Choi, Sci. Rep. 4 (2014) 4225.
[26] J. Kim, S.W. Lee, C. Carlton, Y. Shao-Horn, Electrochem. Solid-State Lett. 14 (2011) B110–B113.
[27] R. Choi, J. Jung, G. Kim, K. Song, Y.-I. Kim, S.C. Jung, Y.-K. Han, H. Song, Y.-M. Kang, Energy Environ. Sci. 7 (2014) 1362–1368.
[28] J.K. Nørskov, J. Rossmeisl, A. Logadottir, L. Lindqvist, J.R. Kitchin, T. Bligaard, H. Jónsson, J. Phys. Chem. B 108 (2004) 17886–17892.
[29] S. Tominaka, M. Shigeto, H. Nishizeko, T. Osaka, Chem. Commun. 46 (2010) 8989–8991.
[30] X. Peng, Y. Zhao, D. Chen, Y. Fan, X. Wang, W. Wang, Electrochim. Acta 136 (2014) 292–300.
[31] M. Ammam, E.B. Easton, J. Power Sources 222 (2013) 79–87.
[32] P.E. Blöchl, Phys. Rev. B 50 (1994) 17953–17979.
[33] G. Kresse, J. Furthmuller, Phys. Rev. B 54 (1996) 11169–11186.
[34] J.P. Perdew, K. Burke, M. Ernzerhof, Phys. Rev. Lett. 77 (1996) 3865–3868.
[35] H.J. Monkhorst, J.D. Pack, Phys. Rev. B 13 (1976) 5188–5192.
[36] M. Methfessel, A.T. Paxton, Phys. Rev. B 40 (1989) 3616–3621.
[37] J. Greeley, J.K. Nørskov, Surf. Sci. 601 (2007) 1590–1598.
[38] Y. Ma, P.B. Balbuena, Surf. Sci. 602 (2008) 107–113.
[39] M. Schurmans, J. Luyten, C. Creemers, R. Declerck, M. Waroquier, Phys. Rev. B 76 (2007) 174208.
[40] G. Makov, M.C. Payne, Phys. Rev. B 51 (1995) 4014–4022.
[41] J.S. Hummelshøj, J. Blomqvist, S. Datta, T. Vegge, J. Rossmeisl, K.S. Thygesen, A.C. Luntz, K.W. Jacobsen, J.K. Nørskov, J. Chem. Phys. 132 (2010) 071101.
[42] K.M. Abraham, Z. Jiang, J. Electrochem. Soc. 143 (1996) 1–5.
[43] J.S. Hummelshøj, A.C. Luntz, J.K. Nørskov, J. Chem. Phys. 138 (2013) 034703.
[44] R.F.W. Bader, Chem. Rev. 91 (1991) 893–928.
[45] G. Henkelman, A. Arnaldsson, H. Jónsson, Comput. Mater. Sci. 36 (2006) 354–360.
[46] Y. Hwang, K.-H. Yun, Y.-C. Chung, J. Power Sources 275 (2015) 32–37.